2D and 3D $^{15}N-^{13}C-^{13}C$ NMR Chemical Shift Correlation Spectroscopy of Solids: Assignment of MAS Spectra of Peptides

Chad M. Rienstra,[†] Morten Hohwy,[‡] Mei Hong,[§] and Robert G. Griffin*

Contribution from the Department of Chemistry and Center for Magnetic Resonance, Francis Bitter Magnet Laboratory, Massachusetts Institute of Technology, Cambridge, Massachusetts 02139

Received March 28, 2000. Revised Manuscript Received July 19, 2000

Abstract: Strategies are discussed for resolving and assigning peptide backbone and side chain resonances in uniformly $^{13}C,^{15}N$-labeled solid peptides. Methods for 2D $^{13}C-^{13}C$, $^{15}N-(^{13}C)-^{13}C$, and 3D $^{15}N-^{13}C-^{13}C$ chemical shift correlation spectroscopy are demonstrated in the chemotactic tripeptide N-formyl-[U-$^{13}C,^{15}N$]-Met-Leu-Phe-OH (MLF). Band-selective heteronuclear double-cross polarization (DCP) and γ-encoded homonuclear double-quantum mixing provide large improvements in sensitivity relative to previously published methods. Directional transfers from amide ^{15}N to $^{13}C'$ or $^{13}C^{\alpha}$ resonances provide two- to 3-fold improvements in signal intensity on the observed ^{13}C spin, in comparison to broadband DCP. Similarly, homonuclear $^{13}C-^{13}C$ transfer is enhanced by use of the rotating frame sequence SPC-5; backbone-to-side chain polarization transfers are achieved with especially high efficiency. Furthermore, the double-quantum nature of the homonuclear transfer permits straightforward classification of C', C^{α}, C^{β}, and C^{γ} signals, on the basis of the sign of the cross-peaks. The experiments described here include optimized solid-state analogues of the solution-state schemes commonly employed for amino acid identification and sequential backbone assignment. We expect that these experiments will facilitate application of 2D and 3D correlation methods to assignment of larger solid peptides and proteins.

I. Introduction

The past few years have witnessed a significant expansion in the repertoire of techniques for the study of biomolecules by solid-state NMR.[1] These methods have been applied to problems involving membrane proteins,[2,3] peptide aggregates such as amyloid,[4−6] and enzyme−inhibitor complexes,[7−9] revealing atomic level structural and dynamic information inaccessible to other techniques. In most cases, such experiments have relied on the selective incorporation of ^{13}C or ^{15}N labels at particular sites. The value of such a strategy lies in the ability to directly address specific biochemical questions. This approach has been very successful and is currently the method of choice for addressing a number of problems.

In principle, more efficient methods for measurement of structural constraints may be derived from experiments using uniformly $^{13}C,^{15}N$-labeled (U-$^{13}C,^{15}N$) molecules. This strategy has been essential for spectral assignments and structural studies of larger proteins by solution NMR.[10,11] Such investigations usually employ 2D experiments, such as the $^{1}H-^{15}N$ HSQC,[12] to assess resolution and optimize sample preparation conditions; subsequently, larger 3D and 4D triple-resonance data sets are acquired to identify amino acid types and to establish sequential backbone correlations.[13]

Clearly, such methods would be useful in solids, as well, to increase the rate at which structural and dynamic parameters can be measured. Thus, the problem of assignment and structure determination in U-$^{13}C,^{15}N$ solid biological molecules has recently attracted considerable interest. Partial assignments of selectively and uniformly labeled proteins have been performed with 2D $^{15}N-^{13}C$ and $^{13}C-^{13}C$ spectra, even at relatively low magnetic field strengths (300−400 MHz ^{1}H frequency).[14−17] At high field (750−800 MHz ^{1}H frequency), both the sensitivity

* Corresponding author: GRIFFIN@CCNMR.MIT.EDU or RGG@MIT.EDU.

[†] Current address: Department of Chemistry, Columbia University, New York, NY 10027.

[‡] Current address: Institute for Molecular Biology and Biophysics, ETH-Honggerberg, CH-8093 Zurich, Switzerland.

[§] Current address: Department of Chemistry, Iowa State University, Ames, IA 50011.

(1) Griffin, R. G. *Nat. Struct. Biol.* **1998**, *5*, 508−512.

(2) Creuzet, F.; McDermott, A. E.; Gebhard, R.; van der Hoef, K.; Spijker-Assink, M. B.; Herzfeld, J.; Lugtenburg, J.; Levitt, M. H.; Griffin, R. G. *Science* **1991**, *251*, 783−786.

(3) Marassi, F. M.; Ramamoorthy, A.; Opella, S. J. *Proc. Natl. Acad. Sci. U.S.A.* **1997**, *94*, 8551−8556.

(4) Lansbury, P. T., Jr.; Costa, P. R.; Griffiths, J. M.; Simon, E. J.; Auger, M.; Halverson, K. J.; Kocisko, D. A.; Hendsch, Z. S.; Ashburn, T. T.; Spencer, R. G. S.; Tidor, B.; Griffin, R. G. *Nat. Struct. Biol.* **1995**, *2*, 990−998.

(5) Griffiths, J. M.; Ashburn, T. T.; Auger, M.; Costa, P. R.; Griffin, R. G.; Lansbury, P. T., Jr. *J. Am. Chem. Soc.* **1995**, *117*, 3539−46.

(6) Benzinger, T. L. S.; Gregory, D. M.; Burkoth, T. S.; Miller-Auer, H.; Lynn, D. G.; Botto, R. E.; Meredith, S. C. *Proc. Natl. Acad. Sci. U.S.A.* **1998**, *95*, 13407−13412.

(7) McDermott, A. E.; Creuzet, F.; Griffin, R. G.; Zawakzke, L. E.; Ye, Q. Z.; Walsh, C. T. *Biochemistry* **1990**, *29*, 5767.

(8) Christensen, A. M.; Schaefer, J. *Biochemistry* **1993**, *32*, 2868−2873.

(9) McDowell, L. M.; Klug, C. A.; Beusen, D. D.; Schaefer, J. *Biochemistry* **1996**, *35*, 5395−5403.

(10) Wüthrich, K. *NMR of Proteins and Nucleic Acids*; John Wiley and Sons: New York, 1986.

(11) Wüthrich, K. *Nat. Struct. Biol.* **1998**, *5*, 492−495.

(12) Bodenhausen, G.; Ruben, D. J. *Chem. Phys. Lett.* **1980**, *69*, 185−189.

(13) Cavanagh, J.; Fairbrother, W. J.; Palmer, A. G.; Skelton, N. J. *Protein NMR Spectroscopy: Principles and Practice*; Academic Press: San Diego, 1996.

(14) Straus, S. K.; Bremi, T.; Ernst, R. R. *J. Biomol. NMR* **1998**, *12*, 39−50.

(15) Hong, M.; Jakes, K. *J. Biomol. NMR* **1999**, *14*, 71−74.

(16) Hong, M. *J. Magn. Reson.* **1999**, *139*, 389−401.

(17) Hong, M. *J. Biomol. NMR* **1999**, *15*, 1−14.

10.1021/ja001092v CCC: $19.00
Published on Web 10/24/2000

and resolution of protein spectra improve significantly, permitting the assignment of many residues in 2D $^{13}C-^{13}C$ experiments.[18,19] To obtain complete and unambiguous sequential assignments, backbone $^{13}C'-^{15}N-^{13}C^{\alpha}$ correlations must be measured, which requires refinement of methods for correlation spectroscopy in solid U-^{13}C,^{15}N peptides and proteins. In particular, solid-state experiments currently rely on direct detection of signals from low-γ nuclei (usually ^{13}C or ^{15}N), and this leads to a factor of 10−50 lower sensitivity than would in principle be available via ^{1}H detection, if sufficiently narrow ^{1}H signals could be observed (see Section III,b below).

Recently, 2D $^{15}N-^{13}C$[20,21] and 3D $^{15}N-^{13}C-^{13}C$[22] chemical shift correlation experiments in solids were investigated; the amino acids U-^{13}C,^{15}N-His and U-^{15}N,^{13}C-Arg were investigated, yielding results relevant to systems with a relatively high ratio of ^{15}N:^{13}C spins (∼1:2). In most peptides, however, the ratio of ^{15}N:^{13}C spins is lower (∼1:4), so for the general case, one must consider in greater detail approaches to optimally transfer polarization from the ^{15}N to the ^{13}C reservoir. In addition, the chemical shift dependence of the homonuclear polarization transfer must be considered and its deleterious effects minimized to produce maximal $^{13}C-^{13}C$ cross-peak intensity.

Here we examine the spin dynamics in peptide topologies by employing the chemotactic tripeptide formyl-Met-Leu-Phe-OH (MLF),[23,24] which is well-suited for these studies for several reasons. First, although a crystal structure of the methyl ester (MLF−OMe) is available[25] and the acid form studied here is readily prepared in a microscopically well-ordered state, crystals suitable for diffraction have not been obtained (E. Gavuzzo, personal communication). Thus, the conformation for this form of the molecule is not known. Second, the absence of side chain protection chemistry permits efficient synthesis of ^{15}N,^{13}C-labeled MLF by standard solid-phase methods. Third, microcrystalline MLF is sufficiently well-ordered so that inhomogeneous broadening due to chemical shift dispersion is less than 0.2 ppm, and the ^{13}C and ^{15}N chemical shifts are well-dispersed. Fourth, the sample is stable at room temperature and has, like most solid peptides, a short ^{1}H T_1, so relatively rapid repetition rates (recycle delays of 2.5 s or less) are routine.

Our experiments in MLF demonstrate that ramped, band-selective (SPECIFIC)[26] double-cross polarization (DCP)[21,27,28] permits the efficient, directional transfer of polarization from amide ^{15}N signals to $^{13}C'$ or $^{13}C^{\alpha}$, yielding up to 3-fold increases in sensitivity relative to broadband DCP experiments. This directional transfer permits interresidue (N[i]−C′[i−1]) and intraresidue (N[i]−C$^{\alpha}$[i]) correlations to be measured in separate experiments, both of which may be performed faster and with higher sensitivity than the single broadband experiment. For homonuclear $^{13}C-^{13}C$ correlation, the recently developed SPC-5 sequence is employed.[29] This sequence provides broadband γ-encoded[30] homonuclear double-quantum polarization transfer, which is compatible with higher MAS rates than the 7-fold sequences (C7, POST-C7, CMR7)[31−33] while retaining the advantages of minimized dependence on both chemical shifts and dipole vector orientation relative to the rotor frame. In the context of the $^{13}C-^{13}C$ correlation experiment, these characteristics of SPC-5 produce spectra with optimal sensitivity in which the majority of the 2D signal is observed in cross-peaks.

Combining the SPC-5 homonuclear $^{13}C-^{13}C$ mixing with the band-selective SPECIFIC $^{15}N-^{13}C$ DCP transfer results in an optimized 3D $^{15}N-^{13}C-^{13}C$ correlation experiment. With this method, MLF 3D spectra having excellent sensitivity have been acquired in ∼18 h, where the rate-limiting step is phase cycling. By employing pulsed-field gradients,[34] experiment times could be reduced by an order of magnitude while maintaining more than sufficient sensitivity in small peptides such as MLF. Alternatively, 3D spectra of larger proteins could be acquired in 24−48 h. Thus, we expect the techniques demonstrated here to be useful for assaying conditions of optimal resolution and for deriving sequential chemical shift assignments in solid proteins.

II. Experimental Section

a. Sample Preparation. N-formyl-[U-^{13}C,^{15}N]-Met-Leu-Phe-OH (MLF),[23,24] was prepared from uniformly labeled amino acids (Cambridge Isotope Laboratories, Andover, MA) using standard solid-phase methods and HPLC purification (American Peptide Company, Sunnyvale, CA). Samples for NMR were obtained by slow evaporation from 2-propanol, yielding microcrystals with excellent microscopic order (upon the basis of <0.2 ppm inhomogeneous broadening). Samples were packed in 4-mm rotors (Varian-Chemagnetics, Fort Collins, CO), and solid Teflon end caps wrapped with Teflon tape were inserted into the rotor at liquid nitrogen temperatures in order to ensure a tight room-temperature seal. Under these conditions, MLF is stable indefinitely and has provided spectra with no observable changes in chemical shifts or line widths over many months.

b. NMR Experiments. NMR spectra were acquired using a custom-designed spectrometer (courtesy of Dr. David Ruben) and a triple-resonance transmission line MAS probe[35] operating at a ^{1}H frequency of 500.06 MHz (11.7 T). Solenoid sample coils were mounted in a 4-mm spinner module from Chemagnetics. The U-[^{13}C,^{15}N]-MLF sample (∼15 mg, ∼40 μmol) was packed in the center third of the rotor, over which the rf inhomogeneity was ∼4−6% fwhm.

All experiments employed some version of the generalized pulse sequences presented in Figure 1, with a MAS frequency of 8.9 kHz. Ramped CP from ^{1}H to ^{13}C or ^{15}N created the initial transverse polarization.[36] The direct ^{13}C or ^{15}N magnetization was spin-locked along the CP axis; this resulted in 10−15% increases in total signal

(18) McDermott, A.; Polenova, T.; Bockmann, A.; Zilm, K. W.; Paulsen, E. K.; Martin, R. W.; Montelione, G. T. *J. Biomol. NMR* **2000**, *16*, 209−219.
(19) Pauli, J.; van Rossum, B.; Foerster, H.; de Groot, H. J. M.; Oschkinat, H. *J. Magn. Reson.* **2000**, *143*, 411−416.
(20) Sun, B. Q.; Costa, P. R.; Griffin, R. G. *J. Magn. Reson. A* **1995**, *112*, 191−198.
(21) Baldus, M.; Geurts, D. G.; Hediger, S.; Meier, B. H. *J. Magn. Reson. A* **1996**, *118*, 140−144.
(22) Sun, B. Q.; Rienstra, C. M.; Costa, P. R.; Williamson, J. R.; Griffin, R. G. *J. Am. Chem. Soc.* **1997**, *119*, 8540−8546.
(23) Showell, H. J.; Freer, R. J.; Zigmond, S. H.; Schiffmann, E.; Aswanikumar, S.; Corcoran, B.; Becker, E. L. *J. Exp. Med.* **1976**, *143*, 1154−1169.
(24) Becker, E. L.; Bleich, H. E.; Day, A. R.; Freer, R. J.; Glasel, J. A.; Visintainer, J. *Biochemistry* **1979**, *18*, 4656−68.
(25) Gavuzzo, E.; Mazza, F.; Pochetti, G.; Scatturin, A. *Int. J. Pept. Protein Res.* **1989**, *34*, 409−415.
(26) Baldus, M.; Petkova, A. T.; Herzfeld, J. H.; Griffin, R. G. *Mol. Phys.* **1998**, *95*, 1197−1207.
(27) Schaefer, J.; Stejskal, E. O. *J. Magn. Reson.* **1979**, *34*, 443−447.
(28) Hediger, S.; Meier, B. H.; Ernst, R. R. *Chem. Phys. Lett.* **1995**, *240*, 449−456.
(29) Hohwy, M.; Rienstra, C. M.; Jaroniec, C. P.; Griffin, R. G. *J. Chem. Phys.* **1999**, *110*, 7983−7992.
(30) Nielsen, N. C.; Bildsøe, H.; Jakobsen, H. J.; Levitt, M. H. *J. Chem. Phys.* **1994**, *101*, 1805−1812.
(31) Lee, Y. K.; Kurur, N. D.; Helmle, M.; Johannessen, O. G.; Nielsen, N. C.; Levitt, M. H. *Chem. Phys. Lett.* **1995**, *242*, 304−309.
(32) Hohwy, M.; Jakobsen, H. J.; Edén, M.; Levitt, M. H.; Nielsen, N. C. *J. Chem. Phys.* **1998**, *108*, 2686−94.
(33) Rienstra, C. M.; Hatcher, M. E.; Mueller, L. J.; Sun, B.-Q.; Fesik, S. W.; Herzfeld, J.; Griffin, R. G. *J. Am. Chem. Soc.* **1998**, *120*, 10602−10612.
(34) Maas, W. E.; Laukien, F. H.; Cory, D. G. *J. Am. Chem. Soc.* **1996**, *118*, 13085−13086.
(35) McKay, R. A. *Encyclopedia of Magnetic Resonance*; 1996; pp 3768−3771.
(36) Wu, X.; Zilm, K. W. *J. Magn. Reson. A* **1993**, *104*, 154−165.

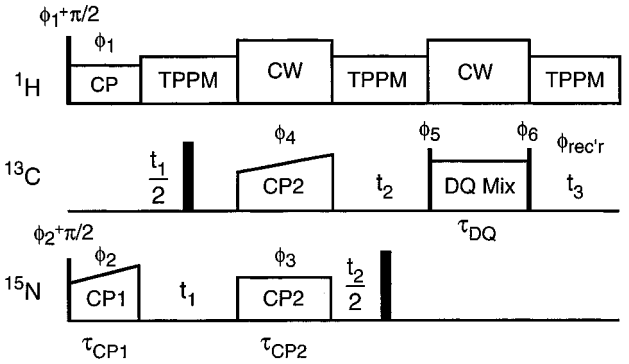

Figure 1. Pulse sequence for 3D $^{15}N-^{13}C-^{13}C$ correlation spectroscopy. Narrow and wide solid rectangles represent $\pi/2$ and π pulses, respectively. Heteronuclear polarization transfer by ramped SPECIFIC CP may be directed within or between residues by choice of ^{13}C rf frequency and field amplitude (see text for further details). The DQ mixing sequence (SPC-5,[29] POST-C7,[32] or CMR7[33]) is chosen for optimal performance at the desired MAS rate and decoupling conditions; SPC-5 was used in all cases shown here. Optional delays of one rotor period were inserted between the bracketing $\pi/2$ pulses and the DQ mixing, and the ^1H decoupling field was reduced during this time to attenuate residual transverse magnetization. Phase cycling was performed as follows, where $\phi_i = J_i * \pi/2$: $J_1 = 1$, $J_2 = 13$, $J_3 = 1$, $J_4 =$ 11111111 33333333, $J_5 = 2$, $J_6 =$ 11223344, and $J_{rec'r} =$ 1324 3142 3142 1324. Hypercomplex data was acquired by shifting ϕ_2 and ϕ_4 according to Ruben and co-workers.[38] Additional phase cycling of ϕ_3 and ϕ_5 may improve quadrature image suppression in cases in which low-γ nuclei have rapid T_1 relaxation. Spin temperature alteration of ϕ_1 (13) is not necessary and in practice results in 10−15% signal intensity losses as compared to the scheme shown here.

intensity relative to CP alone due to the relatively short ^{13}C and ^{15}N T_1 and ^1H $T_{1\rho}$ relaxation times. Spin-locking fields were ∼65 kHz for ^1H and ramped from 52 to 58 kHz for ^{15}N and ^{13}C; contact times were 700−850 μs. The total CP intensity demonstrated a strong dependence both on the amplitude of spin-locking fields and the contact time in MLF at room temperature. In particular, $^1H-^{15}N$ CP efficiency approximately doubled upon increasing $\omega_{1N}/2\pi$ from ∼35 to ∼55 kHz. Particularly short (200−300 μs) $T_{1\rho}$ values in the Phe aromatic region (due, presumably, to intermediate-to-fast-rate ring flipping) resulted in nonoptimal CP efficiency for those resonances. Chemical shift evolution periods incorporated TPPM decoupling.[37] The optimized values for pulse width and total phase difference were 5.3 μs and 10°, using a ^1H rf setting appropriate for a 5.7-μs steady-state π pulse (∼88 kHz nutation field).

The heteronuclear transfers were achieved using a ramped version of SPECIFIC DCP,[26] using a constant ^{15}N rf field amplitude and linear ramp of the ^{13}C rf amplitude from ∼2−3 kHz below to ∼2−3 kHz above the range of desired DCP conditions. In all cases, the ^{15}N carrier frequency was centered in the amide ^{15}N region (in this case, ∼115−120 ppm). The ^{15}N rf field amplitude, ^{13}C carrier frequency, and ^{13}C rf amplitude were optimized to emphasize particular DCP conditions, as detailed in Table 1.

These conditions were optimized first by considering the theoretical matching profile (as reviewed below) and careful measurements of rf field distributions by nutation experiments on both ^{15}N and ^{13}C. A relatively large ^{15}N field amplitude ($\omega_{1N} \gg \Omega_N$) was chosen so that all ^{15}N resonances experienced the same effective field. For the broadband $^{15}N-^{13}C$ 2D experiments discussed below (**I** and **II**), the ^{13}C carrier frequency was approximately centered between the C′ and C^α regions. For the band-selective experiments (**III** and **IV**), the ^{13}C carrier frequency was offset by 30−50 ppm in the direction of the desired destination spins. The amplitude of the ^{13}C rf field was chosen so that the C′ and the C^α/C^β bandwidths experienced effective fields differing by approximately half the MAS frequency. Greater selectivity may be achieved by placing the ^{13}C carrier farther from the center of the spectrum at the cost of reduced efficiency during the homonuclear DQ mixing period. (Improved combinations of band-selective DCP and broadband SPC-5 may be achieved by coherent frequency switching during the mixing periods, but such schemes were not explored here.) The amplitude of the ^{13}C field was incremented stepwise so that a range of chemical shifts would be matched throughout the mixing period. Some empirical optimization of ramp range and amplitude is generally necessary to account for the distribution of rf fields over the sample volume and to determine an optimal ramp range. Ramping the rf field implies that signals with chemical shifts in the middle of the range will experience the closest approximation to an effective field ramp through resonance.

Table 1. Experimental Parameters for DCP Matching Conditions[a]

cond	emphasis	^{15}N rf ampl (kHz)	^{13}C carrier freq (ppm)	^{13}C rf ampl ramp (kHz)	range of downfield match (ppm)[a]	range of upfield match (ppm)[a]
I	$C^\alpha-C'$	34.0	115	43.0−38.0	95−275	135 to −45
II	$C'-C^\alpha$	34.0	115	21.5−24.5	215−155	15−75
III	$C^\alpha-C^\beta$	30.0	80	19.0−21.5	150−50	10−110
IV	C′	36.5	160	25.5−28.5	240−100	80−220

[a] Upfield and downfield match refer to the ranges of ^{13}C frequencies that satisfy the nearest appropriate dipolar (±1) DCP condition during some portion of the ^{13}C ramp.

Homonuclear DQ transfer was achieved with the SPC-5 mixing sequence.[29] The DQ mixing time (τ_{DQ}) was either 8 or 12 τ_r. Because the SPC-5 supercycle spans 4 τ_r, a multiple thereof is optimal for refocusing chemical shift anisotropy (CSA) interactions with imperfect rf fields. During SPC-5 mixing, resonant CW ^1H decoupling was employed, with a field amplitude optimized via observation of the 1D ^{13}C double-quantum filtered spectrum (with standard phase cycles). Prominent oscillations of the intensities of the ^{13}C DQF spectrum were observed as a function of the ^1H decoupling field,[29] and an optimal level of 106 kHz was employed in all experiments here.

In the 2D and 3D experiments, phase-sensitive detection of the indirect dimensions was achieved using the algorithm of Ruben and co-workers.[38] In most instances, the t_1 and t_2 increments were chosen to be multiples of the MAS frequency, so that folded signals in the under-sampled indirect ^{13}C dimension appear at frequencies of the spinning sidebands in the direct dimension. The selection of MAS frequencies that place the C′ sidebands away from the aliphatic signals therefore implies that the aliased C′ frequencies in the indirect dimension will not overlap with aliphatic resonances. Further details regarding sampling of indirect dimensions and selection of mixing times are included in the figure captions, as are the details of data processing, which in most cases included a modest Lorentzian linebroadening in the indirect dimensions (∼0.2 ppm), followed by a forward linear prediction to double the number of acquired complex data points, a 90°-shifted sine bell apodization function with its zero amplitude at the end of the predicted FID envelope, and an additional zero fill prior to Fourier transformation. Spectral intensities were determined by integration of the line shapes. In reporting transfer efficiency, we assume 100% ^{13}C and ^{15}N labeling. This underestimates the true CP and DQF efficiency due to imperfect isotopic enrichment (specifications for the amino acids are 96−99% ^{15}N and >98% ^{13}C).

III. Results and Discussion

a. Resolution in 1D ^{13}C and ^{15}N Spectra of MLF. Figure 2 shows the primary structure and 1D ^{15}N and ^{13}C spectra of MLF at 500 MHz ^1H frequency. Here we have not employed ^{15}N or ^{13}C decoupling during acquisition, because all ^{15}N, $^{13}C'$, and $^{13}C^\alpha$ signals were resolved in the 1D spectra, even in the presence of heteronuclear scalar couplings. The ^{13}C and ^{15}N chemical shift assignments for MLF (Table 2), which were first determined via 2D $^{15}N-^{13}C$ experiments in a ^{15}N-labeled sample,[39] were confirmed by experiments here.

(37) Bennett, A. E.; Rienstra, C. M.; Auger, M.; Lakshmi, K. V.; Griffin, R. G. *J. Chem. Phys.* **1995**, *103*, 6951−6958.

(38) States, D. J.; Haberkorn, R. A.; Ruben, D. J. *J. Magn. Reson.* **1982**, *48*, 286−292.

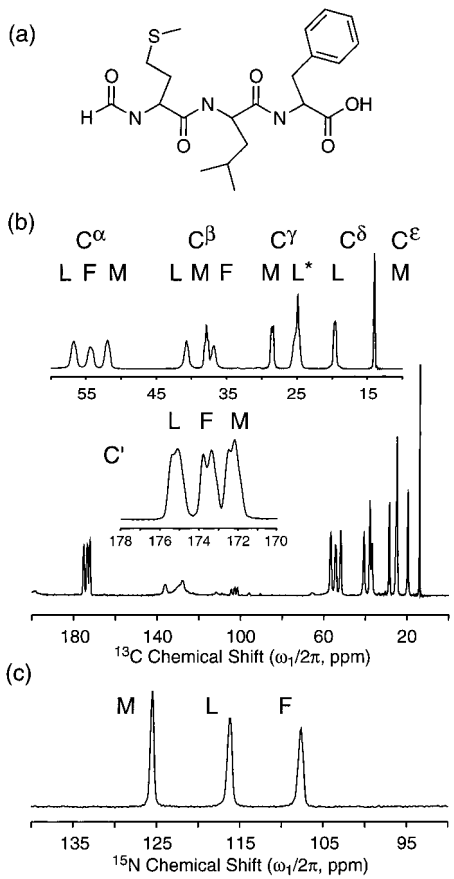

Figure 2. Primary structure and spectra of formyl-[U-^{13}C,^{15}N]Met-Leu-Phe-OH. (a) Primary structure, (b) 1D ^{13}C and (c) ^{15}N CP-MAS spectra of N-formyl-[U-^{13}C,^{15}N]-Met-Leu-Phe-OH (MLF). Spectra were acquired at 500 MHz ^{1}H frequency with 128 transients (2.5-s recycle delay, 5-min total measurement time for each spectrum) using 88 kHz TPPM decoupling (5.3 μsec pulse width, 10° total phase difference) at 8.9 kHz MAS rate, with a 50-ms acquisition time. CP parameters were independently optimized for each spectrum. The ^{13}C spectrum was processed with 5 Hz (0.04 ppm) linebroadening in order to display all signals on the same vertical scale. The ^{15}N spectrum was processed without linebroadening.

Table 2. MLF ^{13}C and ^{15}N Chemical Shift Assignments[a]

residue	N	C′	Cα	Cβ	Cγ	Cδ
Met	125.5	172.2[b]	52.0	37.9	28.6	14.0
Leu	116.2	175.2	56.8	40.7	25.6	24.9, 19.6
Phe	107.6	173.5	54.4	36.9	136.2	128.1[c]

[a] Chemical shifts are referenced to TMS using adamantane as a secondary ^{13}C standard (38.56 ppm $^{13}CH_2$ and 29.50 ^{13}CH). The virtual liquid $^{15}NH_3$ zero point is calculated from the standardized gyromagnetic ratios of ^{15}N and ^{13}C.[92,93] Uncertainties are ±0.1 ppm. [b] The natural abundance formyl C′ signal resonates at 165.3 ppm. [c] The broad, upfield portion of the Phe aromatic region is peaked at this value.

Several features in the spectra are notable. First, all of the line widths of individual signals are less than 1 ppm. The ^{1}H−^{13}C dipolar and scalar couplings have been greatly reduced by TPPM decoupling.[37] Here, the TPPM pulse width (5.3 μs) and phase difference (10°) have been carefully optimized with 88 kHz steady-state ^{1}H fields. Independent optimizations at 80 kHz and 100 kHz result in line widths differing by less than ∼2−3 Hz from those observed here (for ^{13}Cα signals) and slightly more (∼5 Hz) for the $^{13}CH_2$ signals, indicating that the remaining contribution from the ^{1}H−^{13}C dipolar couplings is a small fraction of the total line width (Table 3). Explicit line-shape simulations (not shown), which include the one- and two-bond scalar couplings, result in a fitted Lorentzian broadening of ∼5−10 Hz for the ^{13}C′ and $^{13}CH_3$ signals, 15−20 Hz for the ^{13}CH signals, and 20−30 Hz for the $^{13}CH_2$ signals. Thus, we conclude that some additional narrowing can be expected at higher decoupling field amplitudes, but the convergence to zero residual coupling is slow over this regime.

Table 3. MLF 1D ^{13}C and ^{15}N Spectral Resolution and Sensitivity

signal	line width (Hz, ppm)	signal-to-noise ratio[a]	line width (Hz)* S/N ratio[b]
Met Cα	103, 0.82	600	61900
Leu Cα	110, 0.88	580	63600
Phe Cα	121, 0.97	460	55600
Leu Cβ	86, 0.68	590	50200
Met Cγ	67, 0.54	860	57600
Leu Cδ1	60, 0.48	1000	59900
Met Cδ	27, 0.22	2190	59700
Met N	25, 0.49	345	8450
Leu N	34, 0.67	265	8880
Phe N	35, 0.71	233	8260

[a] Signal-to-noise ratio for a 128-scan CP-MAS experiment (2.5-s recycle delay; total measurement time, 5 min.) at 8.9-kHz MAS rate. [b] For the ^{13}C listed here, the sensitivity factor is 58300 ± 4500; for ^{15}N, 8500 ± 300. The ratio of 6.85:1 is consistent with an overall receptivity proportional to $(\gamma_C/\gamma_N)^{2.1}$.

Additional features of the 1D ^{13}C spectrum include the broad aromatic Phe resonances (due to ring flipping and scalar couplings comparable to the chemical shift differences) and the natural abundance signal from the formyl C′ group. The narrowest line width (of the upfield Met ^{13}Cε resonance) is <0.2 ppm, which places an upper bound on the contribution of chemical shift dispersion and anisotropic bulk magnetic susceptibility to the line widths.[40] This is a typical inhomogeneous line width for dilute ^{13}C and ^{15}N spins in well-ordered microcrystalline powders[41−43] and compares well with typical ^{13}C and ^{15}N line widths of proteins in solution.

In addition to the heteronuclear decoupling and inhomogeneous broadening mechanisms, in U-^{13}C,^{15}N-labeled samples, scalar couplings and residual homonuclear dipolar couplings (due to the proximity to rotational resonance, R^2, conditions)[44,45] may also contribute significantly to the total line width. Here the MAS frequency of 8.9 kHz avoids strong R^2 conditions, leaving primarily the homonuclear scalar couplings as the determinants of ^{13}C resolution. This contribution (∼55 Hz for C′−Cα and ∼35 Hz for Cα−Cβ scalar couplings) is field-independent and dominates the total line width in microscopically well-ordered materials, provided that adequate ^{1}H decoupling fields and MAS frequencies are employed, which implies that the *absolute* line width may often be independent of magnetic field: for ^{13}Cα, ∼75−125 Hz; for ^{15}N, 25−50 Hz. This expectation is consistent with the observations of recent studies at high field.[18,19]

For several signals, ^{13}C−^{13}C scalar couplings were directly observed in the 1D ^{13}C spectrum, including the carbonyl resonances (most evident in the Phe C′, which has no one-bond ^{15}N-^{13}C coupling), the Met Cβ (a broadened triplet), Met Cγ (doublet) and Leu Cδ (doublet) resonances. The scalar couplings

(39) Hong, M.; Griffin, R. G. *J. Am. Chem. Soc.* **1998**, *120*, 7113−7114.
(40) VanderHart, D. L.; Earl, W. L.; Garroway, A. N. *J. Magn. Reson.* **1981**, *44*, 361−401.
(41) Tounge, B. A. Ph.D. Thesis, Yale University, New Haven, CT, 1998.
(42) Mehta, A. K. Ph.D. Thesis, Yale University, New Haven, CT, 1998.
(43) McGeorge, G.; Alderman, D. W.; Grant, D. M. *J. Magn. Reson.* **1999**, *137*, 138−143.
(44) Levitt, M. H.; Raleigh, D. P.; Creuzet, F.; Griffin, R. G. *J. Chem. Phys.* **1990**, *92*, 6347−64.
(45) Raleigh, D. P.; Levitt, M. H.; Griffin, R. G. *Chem. Phys. Lett.* **1988**, *146*, 71−76.

also contributed to the majority of the line width in the Leu C^{γ} resonance (a broadened quartet-like line shape resulting from one-bond couplings to C^{β}, $C^{\delta 1}$, and $C^{\delta 2}$), which was nearly degenerate with the Leu $C^{\delta 1}$. (The ~6 ppm difference in C^{δ} shifts is due to a γ-gauche effect.)[46] These features indicate that constant-time evolution of the indirect ^{13}C chemical shift dimension(s)[47−49] would significantly improve side chain ^{13}C resolution (in exchange for sensitivity), especially at tertiary carbons in branched-chain amino acids; similar experiments employing scalar decoupling of C^{α} or C′ have been demonstrated to reduce observed line widths for backbone ^{13}C resonances in solid peptides.[14,50]

b. Sensitivity in Multi-Dimensional Solid State Correlation Spectra. In solution NMR, the advantages of indirect detection are well-known.[13,51] However, in solids ,the potential advantage of the higher gyromagnetic ratio ^{1}H spin is in most cases spoiled by very broad ^{1}H line widths (~20 kHz). One recent study demonstrated improved sensitivity with indirect ^{1}H detection of ^{15}N signals in small peptides by employing high field (750 MHz) and spinning rates (29 kHz);[52] however, the improvements were linked to the presumption of broad ^{15}N signals so that no advantage is gained if the ^{15}N line widths are ~0.5 ppm, as is the case in our study. Another recent study considered the choice of ^{15}N or ^{13}C observation in U-^{13}C,^{15}N peptides,[14] in which ^{15}N observation was motivated by the improved resolution of a *J*-decoupled indirect ^{13}C dimension.[50]

Here we did not employ homonuclear $^{13}C-^{13}C$ decoupling and so considered primarily the sensitivity of the 1D ^{13}C and ^{15}N spectra (Table 3) during CP-MAS. $^{13}C-^{13}C$ scalar couplings led to ^{13}C line widths that were 2−5 times greater than ^{15}N line widths, but we still found the signal-to-noise ratio of most resonances were at least a factor of 2 better for ^{13}C than ^{15}N, and for side chain signals with smaller scalar couplings, 3 or more times greater. With ^{13}C decoupling during ^{15}N observation, this difference will be reduced, because the heteronuclear $^{13}C-^{15}N$ scalar couplings account for approximately one-third to one-half of the total ^{15}N line width. In addition to the superior absolute sensitivity, we chose ^{13}C observe because the amide ^{15}N bandwidth is relatively narrow, and digitizing it in the indirect dimension minimizes the number of increments required for our 2D and 3D experiments, in which phase cycling is rate-limiting. An additional argument in favor of ^{13}C observe in the direct dimension is that the $^{13}C^{\beta}$ chemical shift is especially important for resolving and identifying amino acid types,[53] and no solid-state experiments for efficient transfer of polarization from the ^{13}C side chain to the ^{15}N backbone are yet available. To access ^{15}N and $^{13}C^{\beta}$ chemical shifts in the same experiment, polarization initiating on the ^{15}N is most efficiently utilized.

Thus, in the context of the $^{15}N-^{13}C-^{13}C$ experiments, we focused in the following on optimizing sensitivity for multidimensional ^{13}C observe experiments by maximizing the efficiency of polarization transfers. Many high-resolution solid-state 2D $^{13}C-^{13}C$ and $^{15}N-^{13}C$ chemical shift spectra in solids have been published.[20,21,50,54−59] In particular, 2D methods have been used to assign chemical shifts in solid peptides.[39,57,59,60] These experiments have incorporated pulse sequences that are similar to that shown in Figure 1 and that employ initial CP transfer from ^{1}H to one low-γ nucleus, and then one or two periods of indirect chemical shift evolution connected by heteronuclear and/or homonuclear polarization transfer mixing periods. The primary difference has been the polarization transfer method employed. The optimal choice may depend on the MAS rate, the available decoupling power, and the desired bandwidth. Most experiments thus far have utilized broadband heteronuclear polarization transfer methods[21,22,39,61] and RFDR[18,54,55,58−60] or spin diffusion[14,18,62−65] for the homonuclear mixing.

These approaches have been successful in small molecules in which sensitivity is not problematic. However, for investigations of larger molecules, improved transfer efficiency is essential. It is imperative to optimize polarization transfer in each step, especially when multiple transfer steps are involved. This constraint in solids is fundamentally no different from that in solution, although achieving optimal transfer efficiency in solid-state experiments is generally more demanding with respect to probe and spectrometer hardware (especially the available ^{1}H decoupling fields) and the related pulse sequence design.

c. Heteronuclear Polarization Transfer in U-^{13}C,^{15}N Peptides. Heteronuclear polarization transfer may be performed with INEPT-based[66] π pulse methods such as TEDOR.[67] However, because of the orientation-dependent distribution of couplings in a powdered solid, the maximum theoretical transfer efficiency with TEDOR is only ~52%, and in practice, yields are typically only half of that obtained with compensated DCP methods[21,68] or ~25−35% of the directly observed $^{1}H-^{13}C$ spectrum.[15] In U-^{13}C,^{15}N-labeled solids, these results are expected to deteriorate further, due to recoupling of homonuclear dipolar interactions by multiple π pulses, which result in dephasing of transverse ^{13}C polarization due to SEDRA-like DQ and ZQ effects.[54,59,69] The effect of ^{13}C homonuclear couplings can be reduced by applying the majority of π pulses on the ^{15}N channel. However, unless the principal axes of the ^{15}N CSA and $^{15}N-^{13}C$ dipolar couplings are collinear, the recoupled ^{15}N CSA interaction will also cause rapid dephasing of the N_yC_z anti-phase coherence, especially with the relatively large amide ^{15}N CSA.[70] Usually

(46) Barfield, M.; Yamamura, S. H. *J. Am. Chem. Soc.* **1990**, *112*, 4747−4758.
(47) Bax, A.; Mehlkpf, A. F.; Smidt, J. *J. Magn. Reson.* **1979**, *35*, 373−377.
(48) Bax, A.; Freeman, R. *J. Magn. Reson.* **1981**, *44*, 542−561.
(49) Rance, M.; Wagner, G.; Sørensen, O. W.; Wüthrich, K.; Ernst, R. R. *J. Magn. Reson.* **1984**, *59*,
(50) Straus, S. K.; Bremi, T.; Ernst, R. R. *Chem. Phys. Lett.* **1996**, *262*, 709−715.
(51) Ernst, R. R.; Bodenhausen, G.; Wokaun, A. *Principles of Nuclear Magnetic Resonance in One and Two Dimensions*; Clarendon Press: Oxford, 1991; Vol. 14.
(52) Ishii, Y.; Tycko, R. *J. Magn. Reson.* **2000**, *142*, 199−204.
(53) Grzesiek, S.; Bax, A. *J. Am. Chem. Soc.* **1992**, *114*, 6291−6293.
(54) Bennett, A. E.; Ok, J. H.; Griffin, R. G.; Vega, S. *J. Chem. Phys.* **1992**, *96*, 8624−8627.
(55) Boender, G. J.; Raap, J.; Prytulla, S.; Oschkinat, H.; de Groot, H. J. M. *Chem. Phys. Lett.* **1995**, *237*, 502−508.
(56) Baldus, M.; Meier, B. H. *J. Magn. Reson. A* **1996**, *121*, 65−69.
(57) Straus, S. K.; Bremi, T.; Ernst, R. R. *J. Biomol. NMR* **1997**, *10*, 119−128.
(58) Egorova Zachernyuk, T. A.; van Rossum, B.; Boender, G. J.; Franken, E.; Ashurst, J.; Raap, J.; Gast, P.; Hoff, A. J.; Oschkinat, H.; deGroot, H. J. M. *Biochemistry* **1997**, *36*, 7513−7519.
(59) Bennett, A. E.; Rienstra, C. M.; Griffiths, J. M.; Zhen, W.; Lansbury, P. T., Jr.; Griffin, R. G. *J. Chem. Phys.* **1998**, *108*, 9463−9479.
(60) Zell, M. T.; Padden, B. E.; Grant, D. J. W.; Chapeau, M. C.; Prakash, I.; Munson, E. J. *J. Am. Chem. Soc.* **1999**, *121*, 1372−1378.
(61) Michal, C. A.; Jelinski, L. W. *J. Am. Chem. Soc.* **1997**, *119*, 9059−9060.
(62) Suter, D.; Ernst, R. R. *Phys. Rev. B* **1982**, *25*, 6038−6041.
(63) Suter, D.; Ernst, R. R. *Phys. Rev. B* **1985**, *32*, 5608−5627.
(64) Kubo, A.; McDowell, C. A. *J. Chem. Soc., Faraday Trans. 1* **1988**, *84*, 3713−3730.
(65) Tycko, R.; Dabbagh, G. *Isr. J. Chem.* **1992**, *32*, 179−184.
(66) Morris, G. A.; Freeman, R. *J. Magn. Reson.* **1980**, *39*, 163−168.
(67) Hing, A.; Vega, S.; Schaefer, J. *J. Magn. Reson.* **1992**, *96*, 205−209.
(68) Sun, B. Q.; Costa, P. R.; Kocisko, D. A.; Lansbury, P. T., Jr.; Griffin, R. G. *J. Chem. Phys.* **1995**, *102*, 702−707.
(69) Gullion, T.; Vega, S. *Chem. Phys. Lett.* **1992**, *194*, 423−428.

in peptides, the principal axis of the ^{15}N CSA will be oriented 15−20° away from the $^{15}N-^{1}H$ vector,[71] collinear with neither the $^{15}N-^{13}C^{\alpha}$ nor the $^{15}N-^{13}C'$ dipole vectors. Therefore, in practice the combination of $^{13}C-^{13}C$ homonuclear and/or ^{15}N CSA recoupling leads to inferior performance of TEDOR-based sequences in multi-spin systems.

A more appropriate choice for heteronuclear polarization transfer is cross-polarization (CP),[72,73] which is not affected, to first order, by the homonuclear coupling or CSA terms in the Hamiltonian. Schaefer and co-workers developed the original $^{15}N-^{13}C$ DCP experiments for isolated spin pairs.[27,74] To apply extensions of DCP methods to 2D $^{15}N-^{13}C$ correlation spectroscopy, greater bandwidth was required, as first demonstrated with the RFDR-CP sequence.[20] Variable amplitude[75,76] and ramped[36] CP methods were designed primarily to improve $^{1}H-X$ transfer at high MAS frequencies, but they also have relevance to the $^{15}N-^{13}C$ problem. The use of ramped effective fields for $^{15}N-^{13}C$ transfer offers improved efficiency and compensation for rf inhomogeneity and chemical shift offset.[21,22] Recently, Ernst, Meier, and co-workers extensively investigated the dynamics of adiabatic heteronuclear transfer in low-γ two-spin systems.[21,28,77−80] Here we briefly review the essential elements of the spin dynamics, starting with the two-spin Hamiltonian in the rotating frame[81]

$$H = \Omega_I I_z + \Omega_S S_z + \omega_{IS} 2I_z S_z + \omega_{1I} I_x + \omega_{1S} S_x \qquad (1)$$

for which in the general case all terms may be time-dependent. We transform to the tilted frame

$$H = U^{-1} HU \qquad (2)$$

defined by the transformation operator

$$U = \exp[-i(\theta_I I_y + \theta_S S_y)] \qquad (3)$$

in which the inclination angle for each spin is determined by the applied rf field and the frequency offset according to

$$\theta_I = \arctan(\omega_{1I}/\Omega_I), \text{ and } \theta_S = \arctan(\omega_{1S}/\Omega_S) \qquad (4)$$

The magnitude of the effective fields, oriented along the *z*-axis in the new frame, is

$$\omega_{I,\text{eff}} = \sqrt{\omega_{1I}^2 + \Omega_I^2}, \text{ and } \omega_{S,\text{eff}} = \sqrt{\omega_{1S}^2 + \Omega_S^2} \qquad (5)$$

The modulation of spin terms proceeds according to these effective fields, with a second transformation

$$\tilde{H} = U^{-1} HU \qquad (6)$$

for which

$$U = \exp[-i(\omega_{I,\text{eff}} I_z + \omega_{S,\text{eff}} S_z)t] \qquad (7)$$

This time modulation causes all terms to vanish (through first order in average Hamiltonian theory)[82] unless the time-dependence of spin terms resulting from eq 7 is canceled by an equal spatial modulation frequency. This occurs when

$$\omega_{I,\text{eff}} - \omega_{S,\text{eff}} = n\omega_r \qquad (8)$$

In the context of peptide backbone polarization transfer from ^{15}N to ^{13}C, we assume that the ^{15}N carrier frequency is on resonance and that matching conditions may be determined by selecting the ^{15}N (S spin) rf field amplitude and ^{13}C (I spin) amplitude and frequency. Substituting the effective field expressions (eq 5) and solving for the ^{13}C rf amplitude,[26] the required rf amplitude on the I spin may be predicted to be

$$|\omega_{1I}| = \sqrt{(n\omega_R + \omega_{1S})^2 - \Omega_{1I}^2}, n = 0, \pm 1, \pm 2 \qquad (9)$$

Depending on the objective of the experiment, one may choose to maximize or minimize the dependence of the DCP condition on the chemical shift offset term by selection of carrier frequency and rf amplitude parameters. If transfer to a single ^{13}C resonance is desired,[26] small ^{13}C and ^{15}N rf amplitudes are employed in order to accentuate the effect of both chemical shifts. If broadband transfer to all ^{13}C resonances is the goal,[21] then large rf amplitudes are employed and the carrier amplitude and/or frequency of each applied low-γ rf field are swept to match a range of DCP conditions. The intermediate case, in which we prefer to match all ^{15}N amide signals to either the C^{α} or C' regions but equally polarize signals of all residues within the matched bandwidth, is achieved by asymmetric placement of the ^{13}C carrier frequency (i.e., 30−40 ppm away from the center of the spectrum), combined with moderate ^{13}C rf field amplitudes (20−25 kHz). Higher rf amplitudes are utilized on the ^{15}N channel; on the basis of the ∼15−25 ppm chemical shift range (750−1,250 Hz at 500 MHz ^{1}H frequency) in the amide region, which is small compared to the ^{15}N rf field amplitude (34 kHz), all amide ^{15}N spins experience close to the same effective field. Thus, the destination of the polarization is determined primarily by the ^{13}C field parameters. Experiments comparing the transfer efficiency using the various DCP conditions are shown in Figure 3, and relative integrated intensities of several signals are reported in Table 4. To compare the various implementations here, for all experiments the same series of optimization steps were performed. First, a suitable set of DCP matching conditions, based on theory and experimentally determined rf field profiles, was fulfilled; second, rapid rotating frame depolarization due to CSA (rotary resonance recoupling[83]) and/or homonuclear $^{13}C-^{13}C$ recoupling (HORROR[30]) was avoided by shifting both ^{15}N and ^{13}C effective fields away from multiples of the MAS frequency with some empirical optimization; third, other experimental settings, such as decoupling field and mixing time, were optimized iteratively. Under these conditions, the ^{15}N source of polarization limits the

(70) Costa, P. R.; Sun, B. Q.; Griffin, R. G. *J. Am. Chem. Soc.* **1997**, *119*, 10821−10830.
(71) Stark, R. E.; Jelinski, L. W.; Ruben, D. J.; Torchia, D. A.; Griffin, R. G. *J. Magn. Reson.* **1983**, *55*, 266.
(72) Hartmann, S. R.; Hahn, E. L. *Phys. Rev.* **1962**, *128*, 2042.
(73) Pines, A.; Gibby, M. G.; Waugh, J. S. *J. Chem. Phys.* **1972**, *56*, 1776.
(74) Stejskal, E. O.; Schaefer, J.; McKay, R. A. *J. Magn. Reson.* **1984**, *57*, 471−485.
(75) Peersen, O. B.; Wu, X.; Kustanovich, I.; Smith, S. O. *J. Magn. Reson. A* **1993**, *104*, 334−339.
(76) Peersen, O. B.; Wu, X.; Smith, S. O. *J. Magn. Reson. A* **1994**, *106*, 127−131.
(77) Hediger, S.; Meier, B. H.; Ernst, R. R. *Chem. Phys. Lett.* **1993**, *213*, 627−635.
(78) Hediger, S.; Meier, B. H.; Kurur, N. D.; Bodenhausen, G.; Ernst, R. R. *Chem. Phys. Lett.* **1994**, *223*, 283−288.
(79) Hediger, S.; Meier, B. H.; Ernst, R. R. *J. Chem. Phys.* **1995**, *102*, 4000−4011.
(80) Hediger, S.; Signer, P.; Tomaselli, M.; Ernst, R. R.; Meier, B. H. *J. Magn. Reson.* **1997**, *125*, 291−301.
(81) Mehring, M. *Principles of High-Resolution NMR in Solids*, 2nd ed.; Springer-Verlag: Berlin, 1983.
(82) Haeberlen, U.; Waugh, J. S. *Phys. Rev.* **1968**, *175*, 453−467.
(83) Gan, Z. H.; Grant, D. M.; Ernst, R. R. *Chem. Phys. Lett.* **1996**, *254*, 349−357.

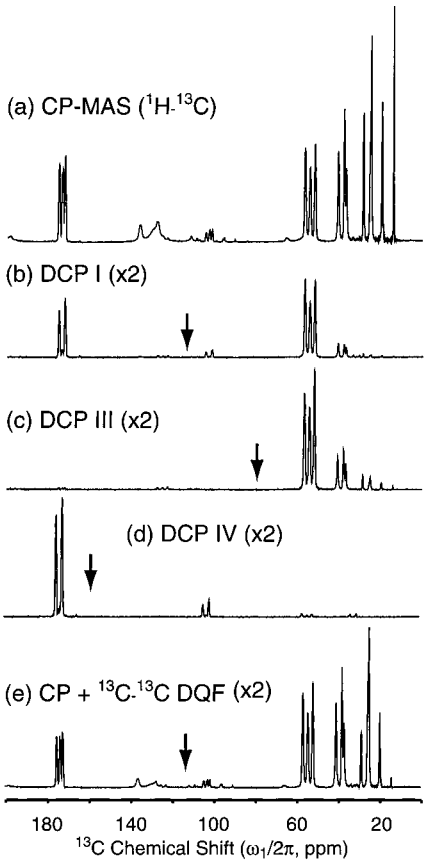

Figure 3. 1D ^{13}C DQF, DCP, and DQF-DCP spectra. Various ^{15}N−^{13}C DCP matching conditions were chosen by setting ^{13}C carrier frequency and amplitude as described in the text. The ^{13}C carrier frequencies are indicated by arrows. (a) CP-MAS reference spectrum (identical to Figure 1); (b) DCP condition I (6 ms), matching both C$^\alpha$ and C′; (c) DCP condition III (10 ms), matching aliphatic region with the majority of transfer to C$^\alpha$ signals; and (d) DCP condition IV (8 ms), matching C′ signals; (e) CP with DQ filtration using SPC-5, with 4 τ_r (0.4446 ms) excitation time. The mixing times were optimized to give maximum total polarization transfer from ^{15}N to ^{13}C for each condition. The total intensity in (e) corresponds to a lower bound for cross-peak intensity in the 2D ^{13}C−^{13}C experiment (discussed in text). Integrated intensities for several signals are shown in Table 4.

Table 4. Relative Intensity of 1D MLF Spectra (CP-MAS, DQF, DCP, and DQF-DCP)[a]

experiment	C′	C$^\alpha$	C$^\beta$	upfield	total[c]
CP-MAS	100	100	100	100	100
DQF	31	50	46	28	35
DCP[b] I and DQF	10	13	6	<1	6
DCP I (C$^\alpha$−C′)	32	40	6	<1	14
DCP II (C′−C$^\alpha$)	49	33	7	<1	15
DCP III (C$^\alpha$)	<1	58	17	2	17
DCP IV (C′)	68	<1	0	0	9

[a] Percentage of polarization observed relative to ^{13}C-observe CP-MAS experiment with CP from ^{1}H. [b] For DCP, only the ^{13}C′ resonances directly bonded to ^{15}N nuclei are considered in the computation of relative efficiency. [c] These values consider all resonances, including the nondirectly bonded C′ resonance and the Phe aromatic ^{13}C signals.

observed ^{13}C signal intensity, and so particular attention was directed toward optimization of the ^{1}H−^{15}N CP step in the context of the DCP experiment.

The spectra were normalized relative to direct ^{1}H−^{13}C CP, and we found that the maximum total ^{15}N−^{13}C polarization transfer did not depend strongly on the direction of transfer; i.e., regardless of whether all C$^\alpha$ and C′ resonances (Figure 3b) or only C$^\alpha$ (Figure 3c) are matched, the total transferred signal intensity was quite similar (14−17% of direct ^{1}H−^{13}C signal) and was approximately equal to the ratio of ^{15}N:^{13}C spins in the molecule (3:20). If only the C′ region was DCP matched (Figure 3d) and, therefore, polarization from only two of the three ^{15}N spins was effectively utilized, 9% (approximately 2:20) of the reference spectrum intensity was obtained. (Because the Phe C′ is not directly bonded to a ^{15}N, there is a gap in the C′ region of all of the DCP spectra.)

Considering individual ^{13}C signals, the intensity observed on ^{13}C nuclei directly bonded to ^{15}N can be ∼60−70% of the direct ^{1}H−^{13}C polarization if each ^{15}N spin is matched to only a single ^{13}C. The relative intensities of signals (Figure 3) within each bandwidth can be rationalized by considering the line widths and number of ^{13}C spins coupled to each ^{15}N. In part a, the intensity patterns were determined mostly by the line widths and, to a lesser extent, by the ^{1}H−^{13}C CP dynamics. All of the Phe residue signals were broader than Leu and Met, which we attribute to residual ^{1}H−^{13}C interactions with the Phe ring protons due to motional interference with ^{1}H decoupling.[84] The intensity pattern among the C′ and C$^\alpha$ signals evident in the direct CP spectrum a was for the most part replicated in parts b, c, and d. In the C′ region, the Met signal (further upfield) gained additional intensity, because among C′ resonances, it receives polarization from both the Leu and the Met ^{15}N, with ∼985 Hz and ∼200 Hz couplings, respectively. The dynamics of band-selective transfer are more straightforward, as shown in parts c and d. The only significant change in the intensity pattern relative to the reference spectrum was the larger Met C$^\alpha$ signal, which we attribute to the fact that only one ^{13}C spin (the Met C$^\beta$) has a ∼200 Hz coupling to the Met ^{15}N, whereas in addition to intraresidue ∼200 Hz couplings, the Leu and Phe ^{15}N signals have additional interresidue ∼200 Hz couplings (to the Met and Leu C$^\alpha$ signals, respectively). Because DCP condition III did not discriminate between C$^\alpha$ and C$^\beta$, the intensity ratio observed was to first order determined by the ratio of the ^{15}N−^{13}C couplings (∼985 to ∼200 Hz).

Whether the ^{15}N polarization is dispersed among all nearby ^{13}C spins or is focused in one direction has clear implications for assignment strategy. In analogy with solution HN[*i*]−C$^\alpha$[*i*]−C$^\beta$[*i*]/C′[*i*][85] and HN[*i*]−C′[*i*−1]−C$^\alpha$[*i*−1][86,87] experiments, intra- or interresidue correlations may be emphasized by choosing one range of CP conditions at a time. For the 2D ^{15}N−^{13}C and ^{15}N−(^{13}C)−^{13}C experiments, band selectivity may decrease spectral overlap and increase sensitivity in the regions of greatest interest. For the 3D experiment, the acquisition time for a required digital resolution is reduced by minimizing the indirect ^{13}C dimension bandwidth. The N−C′ or N−C$^\alpha$ CP conditions generate spectra with >100:1 suppression of undesired C$^\alpha$ or C′ signals, respectively.[88] The ability to control the direction of polarization transfer can be exploited in combination with homonuclear ^{13}C−^{13}C methods as discussed below.

d. Homonuclear Polarization Transfer. Solid-state NMR methods for homonuclear polarization transfer and excitation of homonuclear double-quantum coherence have been developed extensively in recent years. Homonuclear methods benefit from γ-encoded rotating frame approaches that are discussed in several recent publications.[29−33] Due to γ-encoding, the depen-

(84) Rothwell, W. P.; Waugh, J. S. *J. Chem. Phys.* **1981**, *74*, 2721−2732.
(85) Clubb, R. T.; Thanabal, V.; Wagner, G. *J. Magn. Reson.* **1992**, *97*, 213−217.
(86) Bax, A.; Ikura, M. *J. Biomol. NMR* **1991**, *1*, 99−104.
(87) Grzesiek, S.; Bax, A. *J. Magn. Reson.* **1992**, *96*, 432−440.
(88) Wu, X. L.; Burns, S. T.; Zilm, K. W. *J. Magn. Reson. A* **1994**, *111*, 29−36.

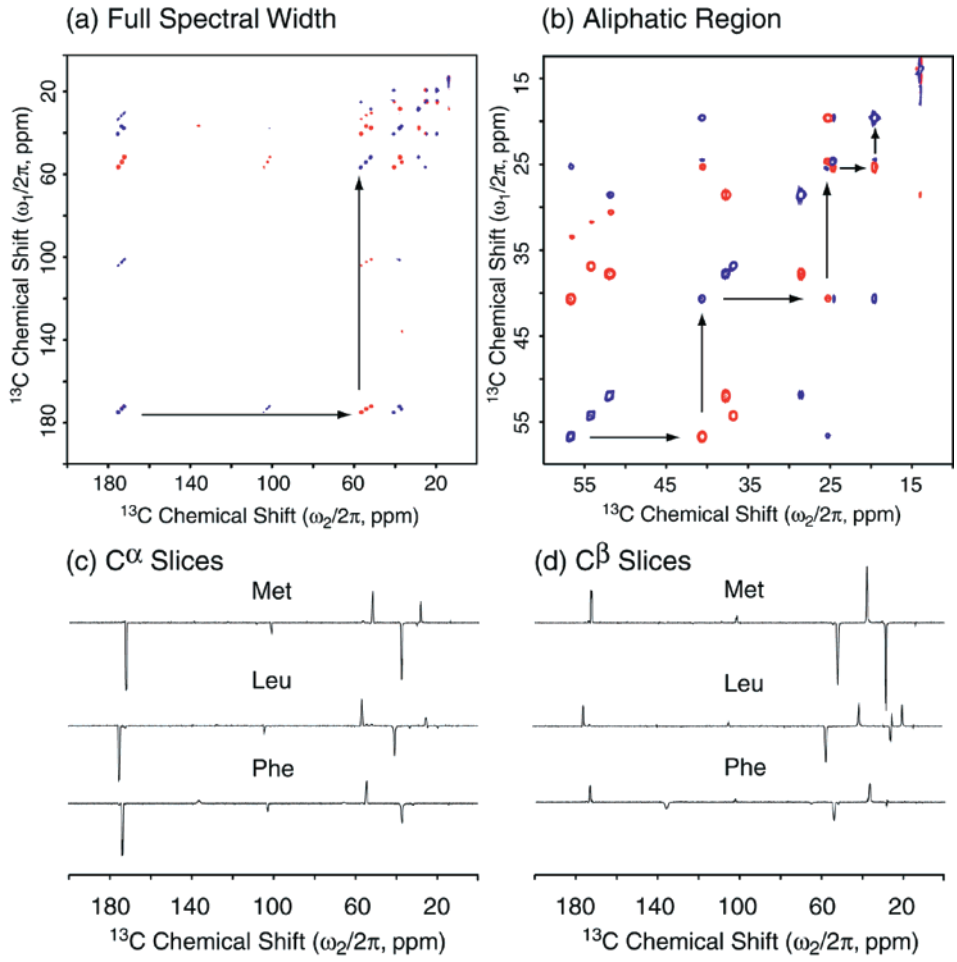

Figure 4. MLF 2D $^{13}C-^{13}C$ correlation spectrum with 12 τ_r (1.3488 ms) SPC-5 mixing time. (a) Full bandwidth; (b) expansion of aliphatic region; (c) slices through the C^{α} resonances in the indirect dimension for each residue (52.0 ppm for Met, 56.8 ppm for Leu, 54.4 ppm for Phe); (d) slices through the C^{β} resonances in the indirect dimension for each residue (37.9 ppm for Met, 40.7 ppm for Leu, 36.9 ppm for Phe). Side chain spin topology can be determined by the sign and frequency of upfield resonances. For the Leu C^{β} slice, partial cancellation near 25 ppm occurred due to the overlap of C^{γ} and $C^{\delta 1}$. The data set was acquired as (512, 2048) complex points in (t_1, t_2) with dwell times of (37.44, 20.0) μs, for net acquisition times of (19.2, 41.0) ms. Each FID was 16 scans, with a 2.5-s recycle delay, yielding a total measurement time of ~12 h. The direct dimension was apodized with a 5-Hz Lorentzian window and zero-filled to 4096 points prior to Fourier transformation (FT). The indirect dimension was apodized (5-Hz Lorentzian) prior to forward linear prediction to 1024 points, 90°-shifted sine bell apodization, and zero-filling to 2048 points for FT.

dence on the powder distribution of crystallites is reduced relative to earlier methods, and broadband sequences such as POST-C7, CMR7, and SPC-5 have an upper threshold of ~73% total polarization transfer in two spin systems. Experimental values of ~70% have been observed with CMR7 in U-^{13}C,^{15}N-Gly.[33] In peptides, with a range of ^{13}C chemical shifts, one of the compensated versions (POST-C7, CMR7, or SPC-5) must be used. We chose SPC-5 because of its superior performance at high MAS frequencies.[29] In 1D spectra, double-quantum filtration (DQF) efficiencies of up to 50% for spins with two neighbors were observed (e.g., C^{α} signals in Figure 3 and Table 4); this is a lower bound on the cross-peak intensity that is expected in the polarization transfer experiments, as is discussed in more detail below.

In principle, the use of the scalar Hamiltonian can remove the dependence on orientation altogether, and techniques have been developed for isotropic scalar transfer, in analogy to TOCSY methods in solution.[56] However, the competition between scalar couplings of 30−60 Hz with typical rotating frame relaxation rates of ~50−100 s^{-1} limits the efficiency of scalar transfers relative to dipolar methods, which exploits couplings of >2 kHz. Even the scaled dipolar coupling (usually 400−500 Hz) derived from a typical windowless mixing sequence is an order of magnitude larger than the scalar coupling. In our hands (at 500 MHz ^{1}H frequency), we observed optimal TOBSY transfer of approximately 10−15%, whereas polarization transfer mediated by the dipolar Hamiltonian often exceeds 50%. The less favorable rotating frame relaxation rates typically observed for many applications (e.g., membrane proteins) will likely increase the advantage of dipolar- versus scalar-mediated transfers. Of course, in systems in which rotating frame relaxation is modest, scalar-mediated transfers may be preferred.

The DQF spectrum in Figure 3e provided ~35% of the entire spectral intensity relative to the direct $^1H-^{13}C$ CP reference. (See Table 4 for a list of DQF efficiencies for each signal type.) The total DQ excitation time of 444.6 μs was chosen in order to minimize the cancellation of polarization due to evolution via multiple $^{13}C-^{13}C$ couplings during DQ reconversion. The spin dynamics involved in this process are explained in greater detail in ref 29. Figure 7 of that reference is an INADEQUATE spectrum of U-^{13}C-alanine, in which weak negative cross-peaks to, for example, the C^{β} frequency in the direct dimension are correlated to the $C'-C^{\alpha}$ DQ coherence in the indirect dimension. This resulted from evolution of the $C'-C^{\alpha}$ DQ coherence under the three-spin Hamiltonian during the reconversion block of the

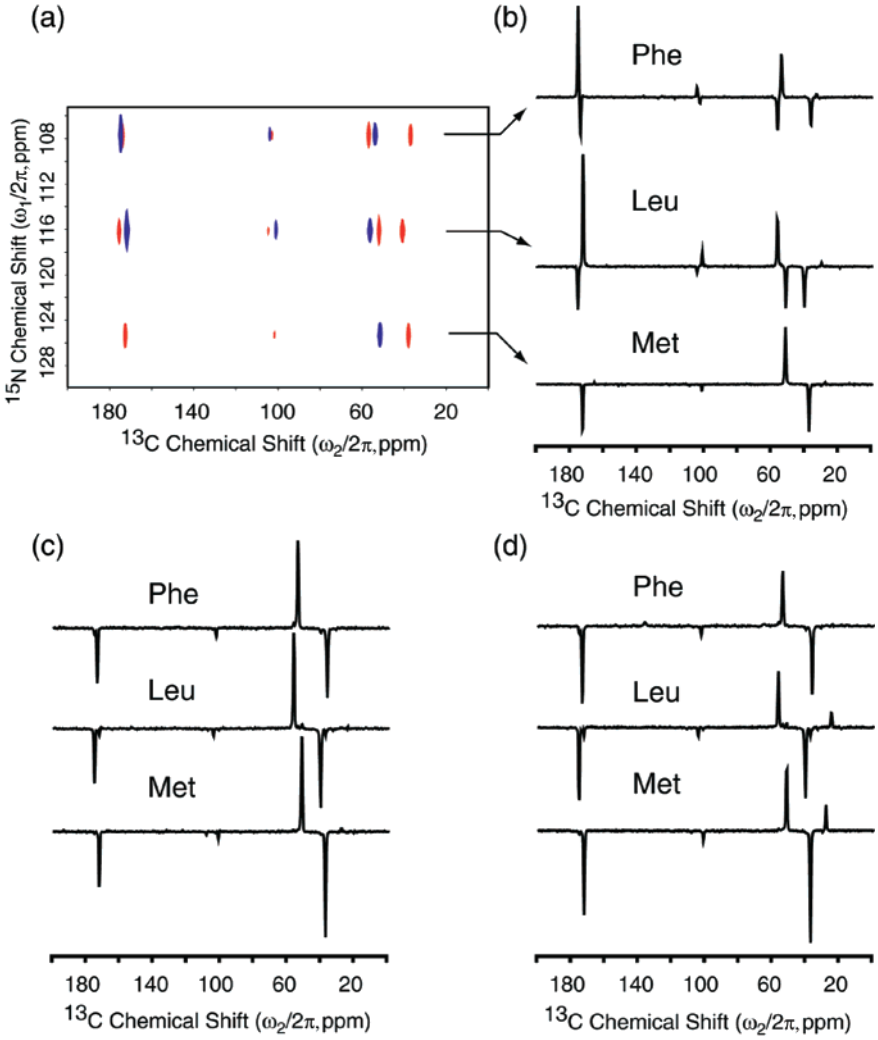

Figure 5. MLF 2D ^{15}N−(^{13}C)−^{13}C correlation spectra. Various DCP and DQ mixing conditions were employed. (a) Broadband, C$^{\alpha}$-emphasized DCP (3 ms, condition I) with 0.8992-ms SPC-5 mixing; (b) C$^{\alpha}$-only DCP (4 ms, condition III) with 0.8992-ms SPC-5 mixing; (c) C$^{\alpha}$-only DCP (4 ms, condition III) with 1.3488-ms SPC-5 mixing. The relatively short, 3−4-ms ^{15}N−^{13}C DCP transfer times were used in order to minimize two-bond (inter-residue N[*i*]-C$^{\alpha}$[*i*−1] and intra-residue N[*i*]−C$^{\beta}$[*i*] and N[*i*]−C′[*i*]) transfer, which would cancel negative DQ-transferred polarization. Data set a was acquired as (32, 2048) complex points with dwell times of (224.64, 20.0) μs, for net acquisition times of (7.2, 41.0) ms. Each FID was 16 scans, with a 2.5-s recycle delay, yielding a total measurement time of ∼45 min. The direct dimension was apodized with a 5-Hz Lorentzian window, zero-filled to 4096, and transformed. The indirect dimension was apodized (10-Hz Lorentzian), doubled with linear prediction, apodized a second time with a 90°-shifted sine bell, and transformed with 128 points. Data sets b and c were acquired as (16, 2048) complex points with dwell times of (449.28, 20.0) μs, for a total measurement time of ∼22 min, and processed in analogous fashion with respect to t_1. The absolute intensity of all spectra has been adjusted according to a single reference spectrum so that peak heights are directly comparable.

sequence. These dynamics are dominated by the ∼2.2 kHz couplings to directly bonded nuclei.[29,89] If the indirect dimension of such an INADEQUATE spectrum were projected (as in the MLF DQF reference spectrum of Figure 3e), partial cancellation of the C$^{\beta}$ peak in the direct dimension would occur. For this reason, the 1D DQF spectrum is a lower bound on the cross-peak intensity in the 2D ^{13}C−^{13}C correlation experiment in which both positive and negative cross-peaks are observed. Polarization transferred over two bonds would result in positive cross-peaks in the 2D DQ-mediated correlation spectrum; this signal cancels in the 1D spectrum. Thus, the 1D DQF spectrum underestimates the total cross-peak intensity by twice the magnitude of the two-step cross-peaks. For this reason, at longer SPC-5 mixing times, the 1D spectra decrease in total observed intensity, but the cross-peak intensities in the 2D spectra increase. Quantitative demonstrations of this effect will be presented elsewhere.

(89) Munowitz, M. *Mol. Phys.* **1990**, *71*, 959−978.

e. 2D ^{13}C−^{13}C Spectra. Figure 4 shows the 2D ^{13}C−^{13}C correlation spectrum of MLF with a 1.3488-ms SPC-5 mixing time. This mixing time, which was slightly longer than that used for the previous DQF 1D spectrum, was utilized in the 2D experiment for reasons discussed above. In MLF, the only significant overlap of negative and positive cross-peaks occurred in the Leu C$^{\gamma}$−C$^{\delta}$ region. In general, peptide spin topology implies that cancellation in the C′−C$^{\alpha}$ and C$^{\alpha}$−C$^{\beta}$ regions will rarely occur, because each first-order cross-peak lies in a distinctive region of the spectrum; this was evident in the full bandwidth spectrum (Figure 4a). Cancellation was more likely among upfield aliphatic resonances (Figure 4b), where overlapping regions of the C$^{\beta}$ and C$^{\gamma}$ shifts are possible. INADEQUATE-type DQ experiments may provide improved resolution and avoid cancellation in this region of the spectrum.[29]

In comparison to 2D RFDR experiments in peptides,[59] superior cross-peak intensities were observed because of the efficiency of the γ-encoded DQ transfer. Particularly large

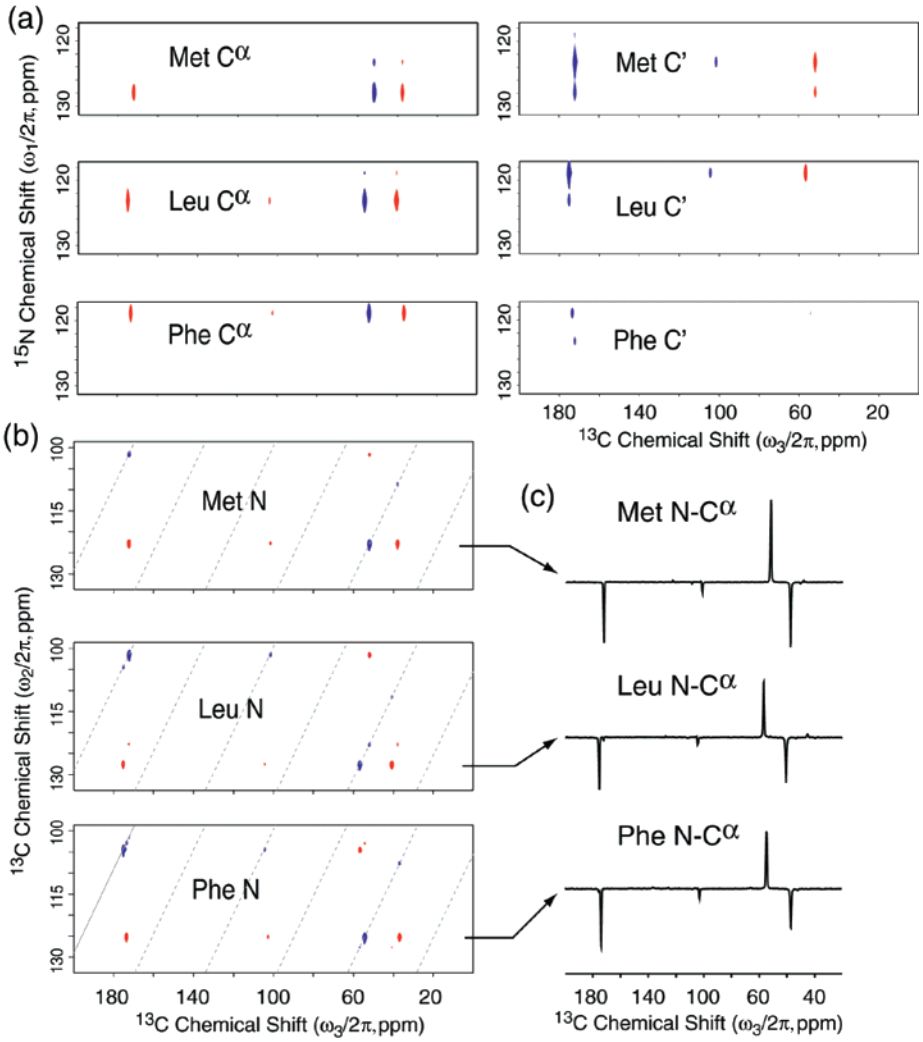

Figure 6. 3D ^{15}N−^{13}C−^{13}C correlation spectrum of MLF. 2D ^{13}C−^{13}C and ^{15}N−^{13}C planes are shown for several ^{15}N and ^{13}C chemical shifts. (a) ^{15}N−^{13}C planes at the Met, Leu, and Phe C$^{\alpha}$ and C′ shifts in $\omega_2/2\pi$; (b) ^{13}C−^{13}C planes at Met, Leu, and Phe ^{15}N shifts in $\omega_1/2\pi$; (c) slices through the N−C$^{\alpha}$ frequencies in $\omega_1/2\pi$ and $\omega_2/2\pi$ for each residue. The (^{15}N)−^{13}C′−^{13}C′ peaks appear in the upper left corner of each ^{13}C−^{13}C plane due to the folding in t_2, indicated by the dotted diagonal lines. DCP condition I was employed (6-ms contact time). The data set was acquired as (12, 32, 1024) complex data points with dwell times of (674.4, 224.8, 25) μs, for net acquisition times of (8.1, 7.2, 25.6) ms. The first t_2 increment was 221.6 μs to ensure zero linear phase due to the storage $\pi/2$ pulse. No such correction is necessary for t_1. Each FID was 16 scans, with a 2.5-s recycle delay, yielding a total measurement time of ∼18 h. The direct t_3 dimension was apodized with a 10-Hz Lorentzian window, zero-filled to 2048 points, and transformed. The indirect ^{13}C (t_2) dimension was apodized with a 20-Hz Lorentzian, doubled by linear prediction, apodized with a 90°-shifted sine bell window, zero-filled to 128 points, and transformed. The indirect ^{15}N (t_1) dimension was apodized with a 10-Hz Lorentzian window, doubled by linear prediction, apodized with a 90°-shifted sine bell window, and transformed (32 points).

improvements were observed in the aliphatic regions, as is illustrated in the C$^{\alpha}$ and C$^{\beta}$ slices (Figure 4c,d). Several slices from signals in the middle of ^{13}C clusters, such as the Met C$^{\alpha}$, Met C$^{\beta}$, and Leu C$^{\beta}$, exhibit >50% of the final intensity in cross-peaks, with ∼15−20% remaining in the diagonal peak and 20−30% lost due to insufficient ^{1}H decoupling during SPC-5. (The polarization loss during mixing was determined through a separate set of 2D experiments as a function of SPC-5 mixing time.) The high overall transfer efficiency is attributable to the fact that the powder-average was over only β_{PR}.

At this mixing time, connectivities over two bonds can easily be distinguished; at least 5% of the polarization originating on each C$^{\alpha}$ and C$^{\beta}$ has been transferred two bonds away, and 13−15% of each initial C′ polarization is transferred via a two-step process to its C$^{\beta}$. In addition to the total efficiency of polarization transfer, the sign of the cross-peaks leads to distinctive patterns that can be used to identify residue type. The sign of the cross-peaks to C′ can help to resolve the ambiguity between C$^{\alpha}$ and C$^{\beta}$ shifts when overlap is possible, primarily among Ser and Thr residues in most proteins. This feature will be especially useful in the 2D ^{15}N−(^{13}C)−^{13}C experiment, in which patterns of shifts may be used to identify amino acid types of both residues.

f. 2D ^{15}N−(^{13}C)−^{13}C Spectra. Combining the ^{15}N−^{13}C DCP and ^{13}C−^{13}C SPC-5 portions of the pulse sequence, with indirect evolution only under the ^{15}N chemical shift interaction, resulted in the ^{15}N−(^{13}C)−^{13}C spectra depicted in Figure 5. The experiment here was implemented using three different mixing conditions. First, broadband DCP (condition I) was used in conjunction with the 8-rotor period SPC-5 mixing time (2D spectrum in Figure 5a and slices through each ^{15}N frequency in Figure 5b). The DCP period was somewhat shorter (3 ms) than that used in the 1D experiments shown above (Figure 3 and Table 4), which resulted in approximately 80−85% of the ^{15}N−^{13}C transfer obtained at longer mixing times. The shorter mixing time was used in order to minimize transfer to intraresidue C$^{\beta}$ and C′, and interresidue C$^{\alpha}$ signals, which would complicate the appearance of each ^{15}N frequency slice. The ratio

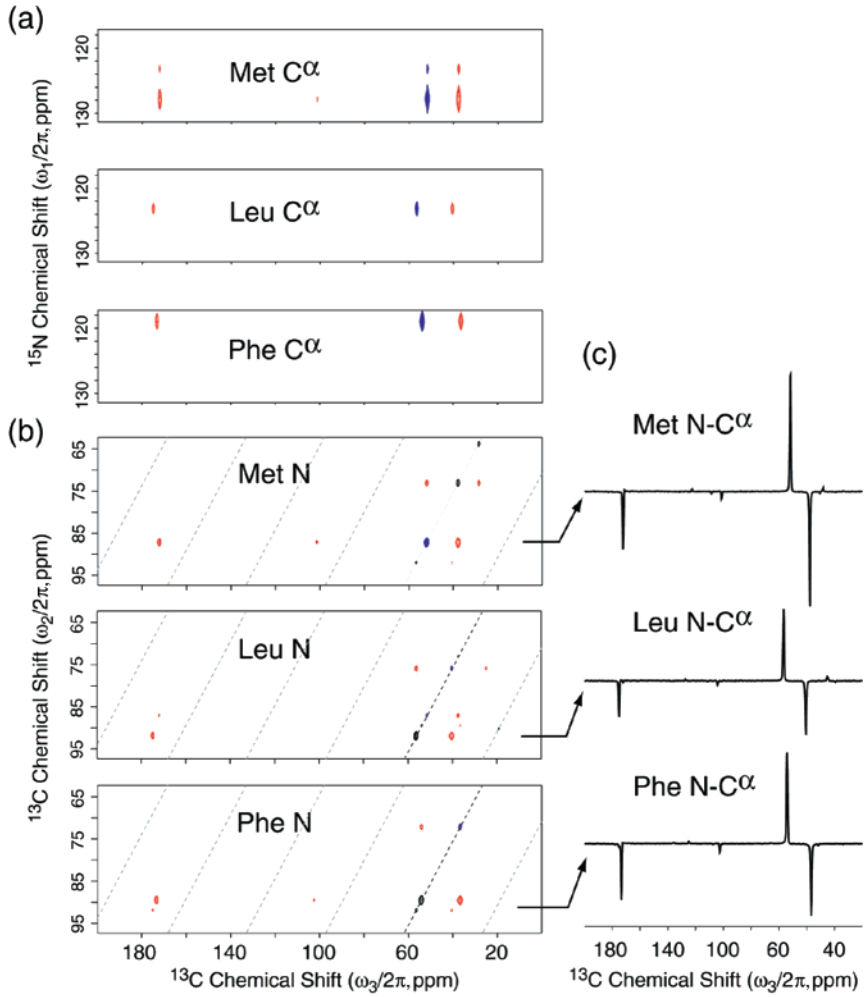

Figure 7. 3D $^{15}N-^{13}C^{\alpha}-^{13}C$ correlation spectrum of MLF. (a) 2D $^{15}N-^{13}C$ planes at $^{13}C^{\alpha}$ frequencies; (b) $^{13}C-^{13}C$ planes at ^{15}N frequencies; and (c) ^{13}C slices at $^{15}N-^{13}C^{\alpha}$ frequencies from the 3D $^{15}N-^{13}C^{\alpha}-^{13}C$ experiment. Conditions were identical to the broadband experiment shown in Figure 8 with the exception of the DCP condition which, in this case, selectively transferred ^{15}N polarization to the aliphatic region (i.e., DCP condition III) with a mixing time of 10 ms. In addition to increases in C^{α}-transferred polarization, C^{β} resonances were polarized directly from ^{15}N. The ^{13}C carrier was placed at 80 ppm. Data sampling and processing routines were identical to those described in the caption of Figure 6.

Table 5. Relative Sensitivity of Signals in 3D Spectra[a]

residue	broadband	band-selective
Met $N-C^{\alpha}-C^{\alpha}$	780 (380)	1390 (540)
Leu $N-C^{\alpha}-C^{\alpha}$	550 (320)	580 (360)
Phe $N-C^{\alpha}-C^{\alpha}$	470 (240)	770 (370)
Met $N-C^{\beta}-C^{\beta}$	130 (60)	340 (180)
Leu $N-C^{\beta}-C^{\beta}$	90 (40)	180 (110)
Phe $N-C^{\beta}-C^{\beta}$	100 (50)	220 (130)

[a] Signal-to-noise ratios (rounded to the nearest multiple of 10) are presented according to data in Figures 6 and 7. The values in parentheses are the signal-to-noise ratios of the same peaks from spectra processed with no linebroadening or linear prediction.

of C^{α}:C′ polarization prior to $^{13}C-^{13}C$ mixing was ~3:2, which was a fortuitous compromise, because the C^{α} polarization transfer was dispersed in two directions and the C′ in only one direction. At the ~900-μs mixing time used here, the C^{α} polarization was divided almost equally among C^{α}, C′, and C^{β}. The C′ resonances were strongly coupled only to a single C^{α} and so less than half of the C′ polarization was transferred. The resulting spectrum showed, in each N[i] slice, positive cross-peaks to C′[$i-1$] and C^{α}[i], and negative cross-peaks to C^{α}[$i-1$], C′[i], and C^{β}[i]. All signals were comparable in intensity. The distinctive pattern of chemical shifts produced in this experiment should be useful for uniquely identifying residue types.[90−93]

The second implementation of the 2D $^{15}N-(^{13}C)-^{13}C$ experiment (slices shown in Figure 5c) involved band selective transfer to C^{α} resonances, using DCP condition III. At the mixing time of 4 ms, little polarization was transferred to intraresidue C^{β} or interresidue C^{α} signals, so that each slice consisted primarily of intraresidue $C'-C^{\alpha}-C^{\beta}$ shifts in the characteristic negative-positive-negative pattern. Transfer to C^{γ} at this SPC-5 mixing time (0.8992 ms) is minimal, but can be improved by increasing the mixing time to 1.3488 ms (Figure 5d). Transfer further out the side chain can be achieved by reducing the amplitude of the ^{13}C rf during SPC-5 (i.e., synchronizing the SPC-5 mixing period to three rotor periods).[29] This experiment resulted in band-selective aliphatic recoupling and will be described elsewhere.

g. 3D $^{15}N-^{13}C-^{13}C$ Spectra. Complete 3D spectra were acquired for both the broadband DCP condition I (Figure 6) and for the band-selective DCP condition III (Figure 7), which

(90) Clubb, R. T.; Thanabal, V.; Wagner, G. *J. Biomol. NMR* **1992**, *2*, 203−210.
(91) Grzesiek, S.; Bax, A. *J. Am. Chem. Soc.* **1992**, *114*, 6291−6293.
(92) Markley, J. L.; Bax, A.; Arata, Y.; Hilbers, C. W.; Kaptein, R.; Sykes, B. D.; Wright, P. E.; Wüthrich, K. *Pure Appl. Chem.* **1998**, *70*, 117−142.
(93) Wishart, D. S.; Bigam, C. G.; Yao, J.; Abildgaard, F.; Dyson, H. J.; Oldfield, E.; Markley, J. L.; Sykes, B. D. *J. Biomol. NMR* **1995**, *6*, 135−140.

required a difference in placement of the ^{13}C carrier frequency. Moving the carrier from 80 to 115 ppm was found to have only a modest effect on the homonuclear polarization transfer profile, owing to the broadband performance of SPC-5, as confirmed by 2D $^{13}C-^{13}C$ spectra preceded by $^{15}N-^{13}C$ transfer with different ^{13}C carrier settings (not shown). Other than the DCP conditions and carrier frequency, experimental and processing parameters for the two 3D spectra were identical. The appearance of the broadband 3D spectra can be appreciated by considering the strips in Figures 6a and 7a in comparison to the 2D spectra shown in Figure 5. The 2D version of the experiment (or equivalently, the $\omega_2/2\pi$ projection of the 3D dataset) shows multiple ^{15}N frequency slices, each coupled to 3−5 ^{13}C signals. Intra- and interresidue C^α and C' signals, though distinguishable by parity, may be nearly degenerate. Indeed, in a more congested spectrum, as expected in larger peptides, overlapping positive and negative cross-peaks are likely.

We show the 3D data as a series of 2D planes at the frequencies of the indirect dimension ^{15}N ($\omega_1/2\pi$) and ^{13}C ($\omega_2/2\pi$) frequencies, as labeled on each plane (C^α and C' planes in Figure 6a, N planes in Figure 6b). Each direct dimension ^{13}C slice at a given ^{15}N frequency is uniquely mapped to the ^{13}C frequency to which the heteronuclear transfer took place. Therefore, each ^{15}N plane displays a single strong positive peak at the $^{15}N-^{13}C^\alpha-^{13}C^\alpha$ frequency, along with negative peaks at $^{15}N-^{13}C^\alpha-^{13}C^\beta$ and $^{15}N-^{13}C^\alpha-^{13}C'$. Other than the small interresidue $^{15}N-^{13}C^\alpha$ transfer resulting in weak cross-peaks, for example, at the Phe(^{15}N)-Leu($^{13}C^\alpha$)-Leu($^{13}C^\alpha$) frequency, the $^{15}N-^{13}C$ slices at each C^α frequency (Figure 6c) are dominated by intraresidue chemical shift patterns and, therefore, are easily interpreted for this simple example. Similarly, interresidue connectivities are immediately evident in the C' planes (Figure 6a). Again, each ^{15}N frequency maps primarily to a single interresidue $^{13}C'$ frequency and appears as a positive peak in the $^{13}C'$ plane along with a negative peak at each $^{15}N-^{13}C'-^{13}C^\alpha$ frequency.

The $^{13}C-^{13}C$ planes at each ^{15}N chemical shift (Figure 6b) show the expected positive cross-peaks to the $C^\alpha[i]$ and $C'[i-1]$ signals and negative cross-peaks to $C^\alpha[i-1]$, $C^\beta[i]$, and $C'[i]$. Each residue also shows a weak, positive cross-peak on the $C^\beta-C^\beta$ diagonal frequency corresponding to intraresidue, two-bond transfer from ^{15}N to $^{13}C^\beta$. The $^{15}N-^{13}C^\alpha$ slices shown in part c of each figure illustrate the absolute sensitivity of the experiments. We found that each $N-C^\alpha-C^\alpha$ signal was enhanced by at least 10%, and in the case of Met, over 100%, in the $N-C^\alpha-C$ experiment relative to the $N-C-C$ experiment. This occurred despite the fact that the longer mixing times of the former experiment transfered a larger fraction of the total polarization to C^β and $C^\alpha[i-1]$ signals. The smaller enhancement of Leu C^α is largely due to the fact that a greater number of ^{13}C nuclei within 3−4 Å of the Leu ^{15}N nucleus (i.e., side chain resonances) are within the bandwidth of DCP condition III. Lower rf fields, faster MAS, and/or shorter mixing times would reduce the distribution of ^{15}N polarization to the Leu side chain and increase the benefit of band-selective transfer for this and similar aliphatic residues.

IV. Conclusions

We have shown that polarization transfer efficiency in multidimensional solid state $^{15}N-^{13}C-^{13}C$ spectra can be enhanced significantly by the use of band-selective heteronuclear polarization transfer and the γ-encoded DQ homonuclear mixing sequence SPC-5. The improvements in the heteronuclear transfer step arose largely from the fact that ^{15}N polarization can be directed to $^{13}C'$ or C^α/C^β spectral regions. In addition, because a smaller ^{13}C rf amplitude was employed in the band-selective $^{15}N-^{13}C$ DCP experiments, experimental conditions could be more effectively optimized, especially with respect to ^1H decoupling. The ordering of $^{15}N-^{13}C-^{13}C$ permitted one transfer step to be homonuclear, which is highly efficient and coherent with γ-encoded SPC-5 mixing, resulting in the majority of the ^{13}C signal being transferred one or two bonds away during the homonuclear mixing. The compatibility of SPC-5 with somewhat higher MAS rates than the compensated C7 analogues POST-C7 and CMR7 assisted in minimizing the loss due to insufficient ^1H decoupling, which in this case was typically 15−20% at ∼0.9 ms and 20−30% at 1.35 ms (least for the $^{13}C'$ and $^{13}CH_3$ signals, greatest for the $^{13}CH_2$ signals). Higher available ^1H decoupling fields would, of course, enhance performance further.

To date, few 3D chemical shift correlation experiments have been implemented in larger solid proteins, despite the potential for improving resolution and facilitating assignment,[17] because of limited sensitivity. These restrictions may be alleviated by the improved polarization transfer efficiency demonstrated here. In addition to the increased signal amplitude of each increment, the overall time required for a 3D experiment may be reduced because only the C^α or C' bandwidth must be digitized in the indirect dimension. Here we used identical sampling of the indirect ^{13}C chemical shift dimension for both the 3D $^{15}N-^{13}C-^{13}C$ and the $^{15}N-^{13}C^\alpha-^{13}C$ experiments, but this choice was strictly to make direct sensitivity comparisons of these spectra. For most applications, the reduced bandwidth of the indirect dimension will permit faster acquisition of a desired digital resolution. In cases in which sensitivity is limiting, as in larger proteins, band-selective transfers will be an even greater advantage. Generally, the ^{15}N bottleneck limits the total transfer to $^{13}C^\alpha$ or $^{13}C'$, and the corresponding cross-peak intensity is reduced by a factor of 2 in the broadband experiment. Assuming this 2-fold sensitivity improvement per unit-time in the band-selective experiment, it will be possible to acquire two separate 3D experiments, $^{15}N-^{13}C^\alpha-^{13}C$ and $^{15}N-^{13}C'-^{13}C$, in the same amount of time as the broadband $^{15}N-^{13}C-^{13}C$ experiment, with $\sqrt{2}$ better sensitivity in each spectrum. The separate experiments emphasizing intra- and interresidue connectivities may be recombined after acquisition for purposes of sequential backbone assignment. These approaches are likely to be used extensively as solid state NMR becomes a mainstream method for structure determination in uniformly labeled proteins.

Acknowledgment. This research was supported by NIH grants RR-00995, AG-14366 and GM-23403. The technical expertise of Dr. David J. Ruben, Ajay Thakkar, Ron Derocher, and Peter Allen was essential for the success of these experiments. We thank Christopher P. Jaroniec for a careful reading of the manuscript. C. M. Rienstra was supported by a Howard Hughes Medical Institute Predoctoral Fellowship, and M. Hong was supported by an NIH Postdoctoral Fellowship (GM-18870).

JA001092V